Electrodynamics of the organic superconductors κ-(BEDT-TTF)$_2$Cu(NCS)$_2$ and κ-(BEDT-TTF)$_2$Cu[N(CN)$_2$]Br

M. Dressel, O. Klein,* and G. Grüner
Department of Physics and Solid State Science Center, University of California, Los Angeles, California 90024-1547

K.D. Carlson, H.H. Wang, and J.M. Williams
Chemistry and Material Science Division, Argonne National Laboratory, Argonne, Illinois 60439
(Received 25 February 1994)

We have performed measurements of the surface impedance in the normal and superconducting states of the title compounds in the millimeter wave-frequency range (1–3 cm^{-1}), and have evaluated the complex conductivity for different crystallographic orientations. Above the transition temperature, the materials behave like metals with a scattering rate of approximately 20 cm^{-1}. In the superconducting state the electrodynamics is in good agreement with calculations based on a BCS ground state: while the penetration depth and the coherence length are anisotropic, the superconducting energy gap shows no indications of line nodes.

I. INTRODUCTION

Among the more than 20 superconducting salts of the organic BEDT-TTF family, where BEDT-TTF is bisethylenedithio–tetrathiafulvalene, κ-(BEDT–TTF)$_2$Cu(NCS)$_2$ and κ-(BEDT–TTF)$_2$Cu[N(CN)$_2$]Br are the ones with the highest transition temperatures at ambient pressure: T_c = 10.4 K and 11.6 K, respectively.[1] In these quasi-two-dimensional compounds, large molecules are coupled to each other forming narrow bands with a low electron density.[2] BEDT-TTF salts contain the almost planar molecules $S_8C_{10}H_4$ which in the κ phase are arranged in dimer pairs with alternating orientations. Separated by polymeric anions of Cu(NCS)$_2^-$ or Cu[N(CN)$_2$]Br$^-$, respectively, the BEDT-TTF molecules form conducting sheets with an interplane separation s of more than 15 Å.[1] For (BEDT-TTF)$_2$Cu(NCS)$_2$, the room temperature conductivity of the highly conducting (bc) plane is about 20 $(\Omega\,\mathrm{cm})^{-1}$with an in-plane anisotropy σ_c/σ_b of approximately 2 and an out-of-plane ratio σ_c/σ_a larger than 600.[3,4] (BEDT–TTF)$_2$Cu[N(CN)$_2$]Br has a slightly different crystal structure than (BEDT-TTF)$_2$Cu(NCS)$_2$, resulting in different unit cell sizes and symmetries.[1] In accordance with the standard setting of the space group symbol, the interlayer cell direction in (BEDT-TTF)$_2$Cu[N(CN)$_2$]Br is b and the conducting planes of BEDT-TTF molecules are (ac). The room temperature conductivity of (BEDT–TTF)$_2$Cu[N(CN)$_2$]Br is comparable to the one of (BEDT–TTF)$_2$Cu(NCS)$_2$: $\sigma_{ac} = 20\ (\Omega\,\mathrm{cm})^{-1}$ and $\sigma_b = 2\times10^{-2}\ (\Omega\ \mathrm{cm})^{-1}$.[5]

Various experiments examining the superconducting state of the BEDT-TTF materials, mainly conducted on (BEDT-TTF)$_2$Cu(NCS)$_2$, indicate deviations from what is expected for singlet pairing. The critical field H_{c2} shows an unexpected behavior at low temperatures[6] and does not follow the linear dependence predicted by the Ginzburg-Landau theory. The ^{1}H nuclear spin-lattice relaxation rate $1/T_1$ was found[7–9] to have an anomalous peak at half T_c. Some measurements[10] of the specific heat exhibit a strange T^3 law at very low temperatures with no residual linear-T contribution, and an unusual bending right below T_c. But others[11] find the specific heat in excellent agreement with the BCS predictions. While both NMR and specific heat measurements are sensitive to excitations other than those of the superconducting state, the parameters which characterize the electrodynamics best, the penetration depth λ and surface resistance R_S, are free from such complications. Consequently, the magnitude and temperature dependences of these parameters may, in principle, distinguish between the various possible symmetries of superconducting states. Low frequency magnetization measurements[8,12] with **H** parallel to the layers exhibit a strong temperature dependence of the penetration depth and lead to an unusually large $\lambda_\parallel$ along the plane and a T^2 dependence suggesting higher momentum pairing. Studies of the reversible magnetization,[13,14] however, show strong evidence of conventional Cooper pairing. From the scaling behavior of the radio-frequency penetration depth, Sridhar *et al.*[15] recently argued for a nonconventional Meissner state where the penetration depth cannot be defined in the common way, and they suggest a flux-flow skin depth. Direct measurements of the penetration depth employing muon spin rotation (μSR) techniques are also highly controversial, one[16] suggesting s-wave pairing, the other[17] showing important deviations from the BCS behavior below 1.5 K. A similar situation has arisen for measurements of the microwave surface impedance. The surface reactance X_S, which is proportional to λ, was found to be temperature independent for $T \ll T_c$ in configurations both parallel and perpendicular to the layers.[18–20] Recently, however, microwave surface impedance experiments were reported[21]

 ©1994 The American Physical Society

which show a slight temperature dependence of the penetration depth down to $0.2T_c$.

After introducing the measurement technique employed in this study, we will present our results on the normal state properties of κ-(BEDT-TTF)$_2$Cu(NCS)$_2$ and κ-(BEDT-TTF)$_2$Cu[N(CN)$_2$]Br followed by the surface impedance, penetration depth, and conductivity in the superconducting state. Parts of the results have been published earlier.[18–20,22–24]

II. EXPERIMENTAL TECHNIQUE AND DATA ANALYSIS

The organic crystals have been prepared by the standard electrochemical crystal growth procedure.[1,25,26] While the (BEDT-TTF)$_2$Cu(NCS)$_2$ samples were typically $1 \times 1 \times 0.1$ mm^3 in size, (BEDT-TTF)$_2$Cu[N(CN)$_2$]Br grows in thicker plates or even blocks of approximately $0.6 \times 0.6 \times 0.5$ mm^3. A routine check of the crystal quality was done by a standard ac susceptibility technique. (The insets of Fig. 1 and Fig. 3 show a typical superconducting transition of (BEDT-TTF)$_2$Cu(NCS)$_2$ and (BEDT-TTF)$_2$Cu[N(CN)$_2$]Br, respectively.) We define the temperature of the superconducting transition at the point where the magnetization signal has changed by 10%. The values of T_c for the (BEDT-TTF)$_2$Cu(NCS)$_2$ samples we measured are typically between 8 and 9 K. The width of the transition is approximately 1 K. The (BEDT-TTF)$_2$Cu[N(CN)$_2$]Br compound has a sharper transition of width ~ 0.3 K and $T_c = 11.3$ K.

To measure the surface impedance $\hat{Z}_S$ in the micro- and millimeter wave range we employed a cavity perturbation technique[27] using resonant cavities at frequencies of 35, 60, and 100 GHz. The cylindrical TE_{011} copper cavities were operated in a transmission configuration; in this mode only circumferencial current flows, making both the field distribution and quality factor Q independent of the contact between the body and the removable end plate. The micro- or millimeter wave power was supplied by either a broadband Impatt source or Gunn oscillator and guided with rectangular waveguides to an input coupling hole on the top plate of the cavity. A diode detector mounted atop a second waveguide measured the power transmitted through the cavity. Both the source and detector were matched to the transmission line with ferrite isolators to avoid standing waves. A broadband mixer, attached to the reference arm of a 10 dB directional coupler, was connected to a frequency counter. An in-line modulator chopped the microwave signal, allowing for lock-in detection techniques. Finally, a Mylar window atop each stainless steel waveguide was used to ensure a vacuum tight environment. A small amount of He exchange gas provided a weak thermal link to the He bath. A complete temperature sweep from 1.5 K to 300 K was possible and one of the probes could be cooled down to ^{3}He temperatures ($T \geq 0.7$ K). The cooling rate was always kept below 1 K/min.

In order to obtain a precise measurement of both the bandwidth Γ and frequency f_0 of the cavity resonance, we have developed a feedback technique which locks the source to the resonance frequency.[28] In this so-called amplitude technique, the source frequency is swept over a very narrow range. The in-phase component of the measured signal is proportional to the difference between the source central frequency and the resonance frequency of the cavity. This correction is fed back to the source to allow a precise tracking of the resonance frequency as the temperature varies. For a Lorentzian response, $P(f_0) \propto \Gamma^{-2}$ where $P(f_0)$ is the transmitted power at f_0.

Experiments were conducted by first measuring the temperature dependence of Γ and f of the empty cavity (subscript 0) followed by a subsequent measurement of the same parameters with the sample inside the cavity (subscript S). The complex conductivity $\hat{\sigma} = \sigma_1 + i\sigma_2$ was evaluated from a complex frequency shift by using the standard first order perturbation theory:[27]

$$\frac{\Delta\hat{\omega}}{\omega_0} = \frac{\Delta f}{f_0} + i\frac{\Delta\Gamma}{2f_0} = \frac{f_S - f_0}{f_0} + i\frac{\Gamma_S - \Gamma_0}{2f_0} = -4\pi\gamma\alpha, \tag{1}$$

where α is the polarizability of the sample, and γ is a geometrical factor which depends on the resonator mode used and on the dimensions of both the cavity and the specimen under investigation and has been calculated for an ellipsoidal sample placed at either the maximum electric or magnetic field.[27]

Using the method described above, we were able to reduce the measurement error to $\delta(\Delta\Gamma/2f_0) \approx 3 \times 10^{-7}$ and $\delta(\Delta f/f_0) \approx 3 \times 10^{-7}$ at room temperature and more than a factor of 3 better at low temperature depending on the sample losses.[24]

Two different configurations were employed to measure the ac response in the highly conducting plane of the (BEDT-TTF)$_2X$ crystals. In one configuration, the sample was placed on the bottom of the cavity near the half-radius point, at the maximum magnetic field $\mathbf{H}_{ac}$, and oriented such that the field was perpendicular to the planes. The eddy currents, due to $\mathbf{H}_{ac}$, are within the highly conducting plane. Alternatively, the specimen was placed on a dielectric post in such a way that the maximum electric field $\mathbf{E}_{ac}$ was parallel to the highly conducting plane. Similarly, the out-of-plane properties can be measured by placing the sample in the maximum of the electric field in such a way that the $\mathbf{E}_{ac}$ field is directed normal to the plane. If the magnetic field is oriented within the plane, we also measure the losses perpendicular to the planes.

For specimens where the skin depth $\delta = [2/(\mu_0\omega\sigma_1)]^{1/2}$ is much smaller than the sample dimensions (a condition obeyed over the entire temperature range for the in-plane measurements), the parameter which determines the change of the resonance characteristics upon insertion into the cavity is the surface impedance

$$\hat{Z}_S = R_S + iX_S = \left(\frac{i\mu_0\omega}{\sigma_1 - i\sigma_2}\right)^{1/2}, \tag{2}$$

where μ_0 is the permeability of free space. In this so-called skin-effect (or surface impedance) regime,

$$\frac{\Delta\Gamma}{2f_0} = \zeta\frac{R_S}{Z_0}, \tag{3}$$

$$\frac{\Delta f}{f_0} - C = \zeta\frac{X_S}{Z_0}, \tag{4}$$

with ζ the resonator constant, which depends on the geometry of the surface and its dimensions, and $Z_0 = 377\ \Omega$ the impedance of the free space. The constant C indicates the relative shift from an identically shaped perfect conductor together with an irreproducible frequency shift due to mechanical uncertainties after removing the end plate of the cavity to insert the sample.

In the metallic state, if the single particle relaxation rate $1/(2\pi\tau)$ significantly exceeds the measurement frequency, the experiments are performed in the so-called Hagen-Rubens limit $\omega\tau \ll 1$. In this limit $\sigma_1 \gg \sigma_2$ and $\sigma_1 \simeq \sigma_{dc}$, the dc conductivity. Consequently, from Eq. (2) we obtain

$$R_S = X_S = \left(\frac{\mu_0\omega}{2\sigma_1}\right)^{1/2} = \mu_0\omega\delta/2. \tag{5}$$

Calculating the resonator constant ζ from the geometry of the specimen, we evaluate R_S by Eq. (3), and with Eq. (5) we obtain X_S and subsequently [Eq. (4)] the temperature independent offset C.

In the superconducting state well below T_c the overall temperature and frequency dependence of the surface resistance is given by

$$R_S \propto \frac{\Delta}{k_BT}\left(\frac{\hbar\omega}{\Delta}\right)^2 \ln\left(\frac{\Delta}{\hbar\omega}\right)\exp\left(-\frac{\Delta}{k_BT}\right). \tag{6}$$

At low temperatures where $\sigma_2 \gg \sigma_1$, the surface reactance $X_S(T)$, which is proportional to the measured frequency shift, is proportional to the penetration depth $\lambda(T)$,

$$X_S(T) = \mu_0\omega\lambda(T), \tag{7}$$

and therefore can be directly compared with various model of the superconducting state.

Out-of-plane (BEDT-TTF)$_2X$ are rather poor conductors at high temperatures ($T > 100$ K), and the skin depth δ is much larger than the sample dimension. In this so-called depolarization limit the complex permittivity $\hat{\epsilon} = \epsilon_\infty + 4\pi i\hat{\sigma}/\omega$ for measurements in the antinode of the electric field is given by the quasistatic approximation[29]

$$\hat{\epsilon} = 1 - \frac{\Delta\hat{\omega}/\omega_0}{\gamma + N\Delta\hat{\omega}/\omega_0}, \tag{8}$$

where N is the depolarization factor of the sample and can be calculated for an ellipsoidal shaped specimen.[30] A similar analysis can be done if the sample is placed in the magnetic field maximum.[27]

III. RESULTS AND ANALYSIS

A. Normal state properties

1. κ-(BEDT-TTF)$_2$Cu(NCS)$_2$

The temperature dependence of $2R_S^2/(\mu_0\omega)$ and the dc resistivity along the (bc) plane of κ-(BEDT–TTF)$_2$Cu(NCS)$_2$ are displayed in Fig. 1. The room temperature dc resistivity is around $\rho_{\|} = 0.05\ \Omega$cm. The temperature dependence goes through a small minimum at 250 K and then a broad maximum at 100 K. It drops sharply below this temperature, and in the range 10–30 K it can be fitted by a parabolic function

$$\rho_{\|} = A + BT^2, \tag{9}$$

where $A \approx 5\times10^{-5}\ \Omega$cm and $B \approx 2\times10^{-6}\ \Omega\,\mathrm{cm\,K^{-2}}$. Slightly above the transition (at 10 K) the resistivity is $\rho_{\|} = 2.5\times10^{-4}\ \Omega$cm. $2R_S^2(T)/(\mu_0\omega)$ is also plotted for the results of the microwave measurements at 35, 60, and 100 GHz. This is believed to represent the ac resistivity if $\omega\tau \ll 1$ [Eq. (5)]. The measurements were done on samples from different batches. Studying samples grown in various laboratories (Santa Barbara, Argonne, Orsay) we found that the room-temperature–low-temperature ratio varies, presumably due to impurity concentration and crystal growth conditions. We also observed a correlation between this ratio and T_c, indicating the existence of unintended phases or deviations from the ideal stoichiometry, since it is not obvious why a two-dimensional superconductor is so sensitive to nonmagnetic impurities and defects.[31] This is in agreement with systematic studies.[32,33] Furthermore, it is known that specimen of (BEDT-TTF)$_2$Cu(NCS)$_2$ may decompose with time.[34] Assuming that the low temperature resistivity probes the intrinsic properties, all the data in Fig. 1 were normal-

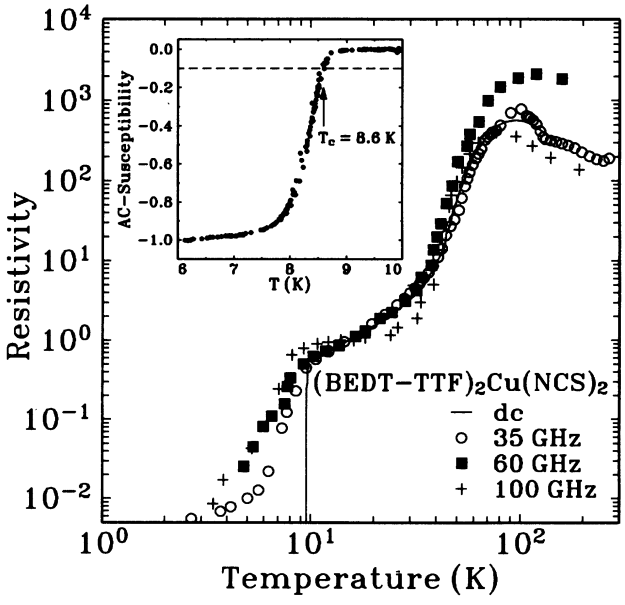

FIG. 1. The temperature dependence of the in-plane resistivity of (BEDT-TTF)$_2$Cu(NCS)$_2$ measured at different frequencies. $R_S^2/\mu_0\omega$ is shown for the millimeter wave data. The curves are normalized to their 15 K value. The inset displays a typical magnitization curve of κ-(BEDT-TTF)$_2$Cu(NCS)$_2$ obtained by ac susceptibility measurements. The superconducting transition temperature $T_c = 8.6$ K is defined by a 10% change of the signal.

ized to their normal state value at $T = 15$ K. Just above T_c our millimeter wave results show no significant frequency dependence within the scattering due to different sample qualities and are in accord with σ_{dc}. We have also observed variations in the transition temperature, as is evident from Fig. 1. The broad transition as seen in the inset is due to a distribution of transition temperatures within the sample. This may be caused by inhomogeneities in the sample and by internal stress, since T_c is strongly pressure dependent.[35] There are no indications of superconducting fluctuations above the nominal T_c. With increasing frequency the surface resistance at the superconducting transition smoothens, as predicted by the BCS theory.[36]

A metal in the Hagen-Rubens regime ($\omega\tau < 1$) has a surface resistance $2R_S^2/(\mu_0\omega) = \rho_{dc}$. In Fig. 1 we notice that $2R_S^2/(\mu_0\omega)$ is equal to the dc resistivity, suggesting that the compound is in the Hagen-Rubens regime. In the normal state at low temperatures (BEDT-TTF)$_2$Cu(NCS)$_2$ is close to a simple metal with a relaxation rate $1/(2\pi\tau_\parallel)$ which exceeds $\omega/2\pi = 3$ cm^{-1} (100 GHz), in agreement with optical studies which lead to a relaxation rate $1/(2\pi\tau_\parallel) \approx 1000$ cm^{-1}.[37] This figure differs a great deal from the value $1/(2\pi\tau_\parallel) = 2$ cm^{-1} obtained by Shubnikov–de Haas experiments.[2] The reasons for this difference are not clear at present and several possible explanations will be discussed below. Nevertheless, assuming the Hagen-Rubens limit applies, we can use the measured value of R_S to estimate the absolute value of the conductivity in the normal state just above T_c [Eq. (5)]: At 60 GHz we obtain a value of $\sigma_{\parallel n}(T = 9\text{ K}) = 3.7 \times 10^3$ $(\Omega\text{cm})^{-1}$ in good agreement with both the dc value[4] $[\sigma_{\parallel n}(T = 12\text{ K}) = 5.0 \times 10^3$ $(\Omega\text{cm})^{-1}]$ and results obtained by far-infrared reflectance measurements[37] $[\sigma_{\parallel n}(T = 10\text{ K}) = 2.0 \times 10^3$ $(\Omega\text{cm})^{-1}]$. The Fermi surface area $S_F = \pi k_F^2 = 6.37 \times 10^{14}$ cm^{-2} and the in-plane effective mass $m^* = 3.5m_e$ obtained from Shubnikov–de Haas and de Haas–van Alphen experiments[2,38,39] lead to a Fermi velocity $v_F = \hbar k_F/m^* = 4.7 \times 10^6$ cm/s in the plane. The charge carrier concentration is $n = 1.6 \times 10^{20}$ cm^{-3} which is significantly smaller than the hole concentration $n = 1.2 \times 10^{21}$ cm^{-3} expected if one carrier exists per formula unit, in agreement with the fact that the Fermi surface contains only 18% of the first Brillouin zone. From this the conductivity leads to a scattering rate of $1/(2\pi\tau_\parallel) = 18$ cm^{-1} and a mean free path $\ell_\parallel \approx 150$ Å. The comparison with other experiments will be done below.

In Fig. 2 we show the temperature dependence of the complex conductivity $\hat{\sigma} = \sigma_1 + i\sigma_2$ in the perpendicular direction, measured at 60 GHz for both experimental configurations: $\mathbf{E}_{ac} \perp (bc)$ plane and $\mathbf{H}_{ac}$ in the plane, respectively. In the latter case, the losses due to the perpendicular direction dominate the contribution of the in-plane resistivity. The insets show the experimentally accessible parameters of the frequency shift $\Delta f/f_0$ and change in bandwidth $\Delta\Gamma/2f_0$ as recorded in the measurement. Although in the normal state the temperature dependence of the raw data is very different for the two configurations, they are supposed to probe the same parameters. For example, the characteristic frequency f_E drops sharply around 50 K while f_H increases. This difference can be explaned through the cavity perturbation theory,[27] in which a sample induces a very different response when the conductivity crosses over from the depolarization to the skin-depth regime, depending on which configuration is employed. By evaluating the complex conductivity, the intrinsic properties show good agreement between the two independent experiments despite the apparent differences in the original experimental results (Fig. 2). This clearly indicates that our assumptions in the evaluation procedure and concerning the current flow are correct.

We estimated $\sigma_{1\perp}(T{=}9\text{ K}) = 4.0$ $(\Omega\text{cm})^{-1}$. Comparing the out-of-plane conductivity to the value of $\sigma_{1\parallel}$ gives an anisotropy of approximately 1.1×10^3. This anisotropy ratio is in agreement with dc values, which range from 600 to 10^3–10^4.[3,4] Despite the large differ-

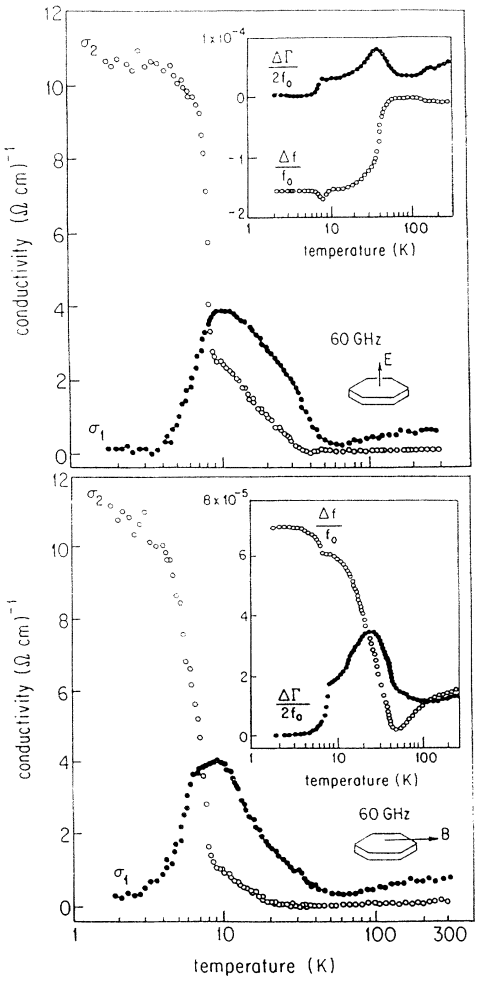

FIG. 2. The temperature dependence of the perpendicular conductivity $\sigma_\perp$ of (BEDT-TTF)$_2$Cu(NCS)$_2$ calculated from the measurement of $\Delta\hat{\omega}/\omega_0$ at the antinode of the electric field is shown in the upper panel. The lower panel shows the results of the measurement done in the antinode of the magnetic field with $\mathbf{H}_{ac}$ in the highly conducting (bc) plane. The raw data $\Delta\Gamma$ and Δf are plotted in the insets.

ence in the absolute value, the temperature dependence of $\sigma_{1\perp}$ is very similar to the one observed for the parallel direction (Fig. 1), e.g., the semiconductorlike behavior at high temperature and a T^2-like drop below 100 K. Using the data shown in Figs. 1 and 2, we have extracted the anisotropy coefficient as a function of temperature, and the ratio $\sigma_{\|}/\sigma_{\perp}$ was found to be almost temperature independent (within 10%) between room temperature and 9 K. This agrees with dc studies[4] where a change in the anisotropy over the entire temperature range by less than a factor 2 was found.

2. κ-(BEDT-TTF)$_2$Cu[N(CN)$_2$]Br

In Fig. 3 the temperature-dependent resistivity of κ-(BEDT-TTF)$_2$Cu[N(CN)$_2$]Br measured at 35 GHz is displayed for both directions, parallel to the highly conducting (ac) plane and normal to it. First the sample was placed in the maximum of the electric field with the highly conducting plane directed parallel to the field (upper panel). In order to probe the out-of-plane properties (lower panel), the sample was put in the antinode of the magnetic field in such a way that the field was oriented within the (ac) plane, inducing some interplane eddy currents. The overall behavior is similar to that observed in (BEDT-TTF)$_2$Cu(NCS)$_2$ (Figs. 1 and 2). Above the broad resistance maximum at about 75 K, the material is semiconducting. Due to lattice contraction the transfer integrals might increase and change the state from a Mott-Hubbard insulator to a metal. $\rho(T)$ drops rapidly between 70 K and 30 K below which it decreases more gradually. At room temperature $\sigma_{\|} = 32\ (\Omega\,\mathrm{cm})^{-1}$ and in this orientation the skin effect limit [Eq. (5)] applies in the entire temperature range. Since the conductivity in the b direction is about two orders of magnitude smaller [$\sigma_{\perp}(T = 300\ \mathrm{K}) = 0.5\ (\Omega\,\mathrm{cm})^{-1}$], the skin effect regime is entered only below 20 K while the data have to be evaluated with the depolarization formulas at higher temperatures.

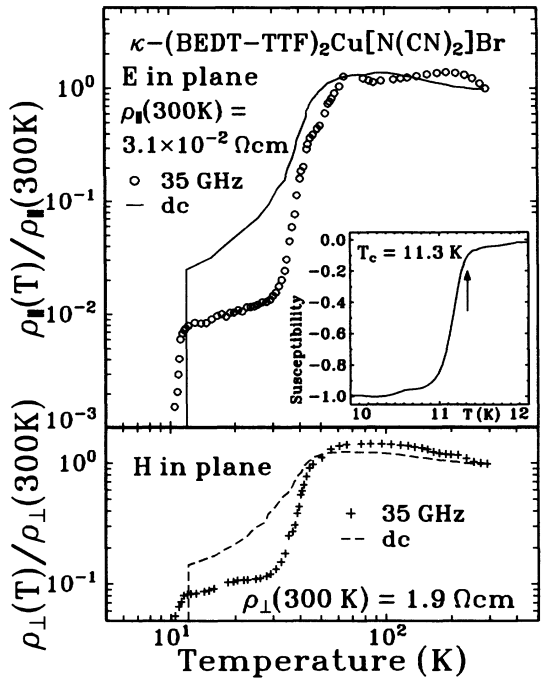

FIG. 3. The upper and the lower panels show the temperature dependence of the resistivity $\rho_{\|}$ and $\rho_{\perp}$ of (BEDT-TTF)$_2$Cu[N(CN)$_2$]Br, respectively, at 35 GHz together with dc results (Ref. 5) normalized to their room temperature values. In the inset ac susceptibility data are displayed in arbitrary units. The superconducting transition at $T_c = 11.3$ K has a width (10% – 90%) of 0.3 K.

The comparison of the 35 GHz results with the dc data of Buravov *et al.*,[5] also shown in the plot, indicates the high quality of our samples since the room temperature to low temperature resistivity ratio is about a factor 4 larger for the microwave results than it is for the dc curve. The deviation can be solely attributed to the different sample quality and it does not indicate a departure from the Hagen-Rubens limit ($\omega\tau < 1$) (σ_1 decreases for $\omega \to \tau^{-1}$). Furthermore, optical studies[40] lead to a low temperature relaxation rate $1/(2\pi\tau) \approx 1000\ \mathrm{cm}^{-1}$ which is far above our measurement frequency $\omega/2\pi = 1.17\ \mathrm{cm}^{-1}$. Slightly above $T_c = 11.3$ K, we obtain $\sigma_{\|n}(T = 13\ \mathrm{K}) = 4.0\times10^3\ (\Omega\,\mathrm{cm})^{-1}$ in excellent agreement with results from extrapolation of far-infrared reflectance measurements[40] [$\sigma_{\|n}(T = 10\ \mathrm{K}) = 4\times10^3\ \Omega\,\mathrm{cm})^{-1}$]. No Shubnikov–de Haas oscillations were observed in (BEDT-TTF)$_2$Cu[N(CN)$_2$]Br but calculations of the band electronic structure[41] yield a Fermi surface similar to that of (BEDT-TTF)$_2$Cu(NCS)$_2$. Therefore using the same charge carrier density, band mass, and Fermi velocity as for (BEDT-TTF)$_2$Cu(NCS)$_2$, we estimate a similar mean free path $\ell_{\|} \approx 150$ Å. Normal to the planes we obtain $\sigma_{\perp n}(T = 13\ \mathrm{K}) = 6.4\ (\Omega\,\mathrm{cm})^{-1}$. The ratio of anisotropy is $\sigma_{\|}/\sigma_{\perp} \approx 650$ at low temperatures, while values of 70 and 5000 have been reported from dc experiments.[5,42]

B. Surface impedance in the superconducting state

1. κ-(BEDT-TTF)$_2$Cu(NCS)$_2$

The temperature dependences of R_S and X_S for (BEDT-TTF)$_2$Cu(NCS)$_2$ at low temperatures are displayed in Fig. 4(a). In this 60 GHz (or 2 cm^{-1}) measurement the electric field $\mathbf{E}_{\mathbf{ac}}$ was parallel to the c direction, and consequently $Z_{S\|}$ is probed. The data were normalized to the value of the surface resistance R_n at 9 K. The most obvious feature of this plot is the sudden drop of R_S below T_c. This is expected for a superconductor for frequencies below the single particle gap 2Δ, for which indications were found around 35 cm^{-1} by tunneling experiments,[43,44] although far-infrared absorption measurements[45] showed no evidence of a superconducting gap down to 10 cm^{-1}. These results can be compared with the BCS prediction[36] $2\Delta = 3.53 k_B T_c = 20\ \mathrm{cm}^{-1}$.

As justified by our further analysis, we find that the limit $\omega\tau \ll 1$ [and therefore Eq. (5)] does not apply

strictly in this temperature and frequency range. Correcting the electrodynamic properties for $\omega\tau \leq 1$ leads to a deviation of both components of the surface impedance from the low frequency limit, as can be seen by a simple expansion

$$R_S = \left(\frac{\mu_0\omega}{2\sigma_{dc}}\right)^{1/2}\left(1 - \frac{\omega\tau}{2} + O[(\omega\tau)^2]\right), \qquad (10)$$

$$X_S = \left(\frac{\mu_0\omega}{2\sigma_{dc}}\right)^{1/2}\left(1 + \frac{\omega\tau}{2} + O[(\omega\tau)^2]\right). \qquad (11)$$

We have fitted the temperature dependence of R_S and X_S for various values of τ leaving the unknown offset C in Eq. (4) as a free parameter. The best fits were obtained for $\omega\tau_{\|} = 0.15$ at 60 GHz [Fig. 4(a)] and $\omega\tau_{\|} = 0.07$ for our 35 GHz results (Fig. 5). Due to the proximity of the measurement frequency of 1 cm^{-1} to the scattering rate

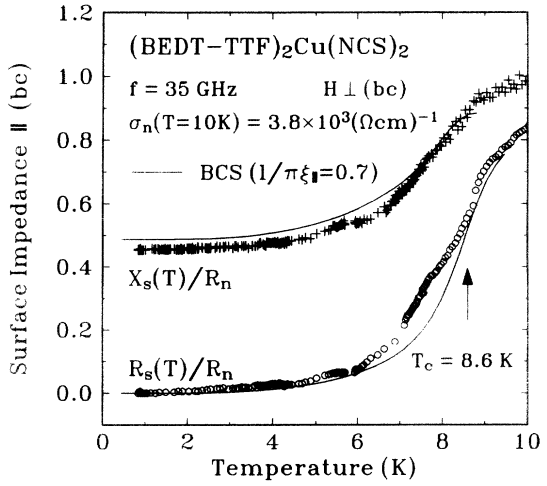

FIG. 5. The temperature dependence of the surface impedance $\hat{Z}_{S\|}$ of $(BEDT\text{-}TTF)_2Cu(NCS)_2$ measured at a frequency of 35 GHz. The experiment was done in the antinode of the magnetic field with $\mathbf{H}_{ac}$ parallel to the (ab) planes.

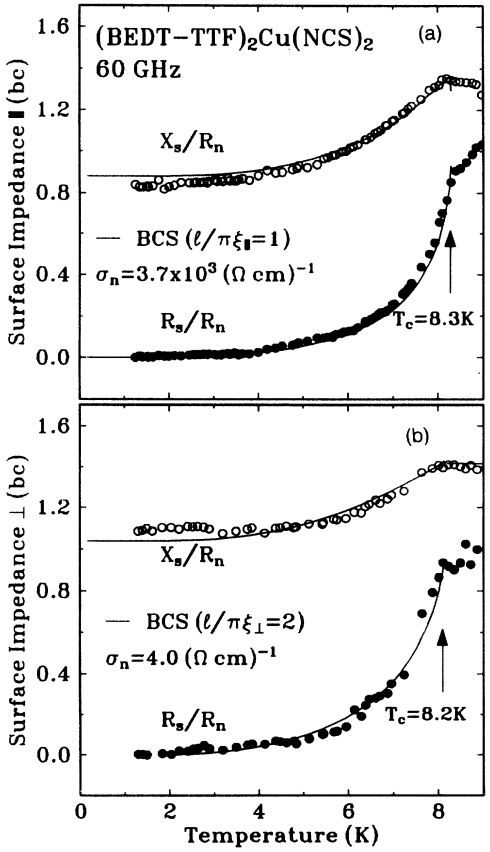

FIG. 4. The surface impedance $\hat{Z}_S$ of $(BEDT\text{-}TTF)_2Cu(NCS)_2$ at 60 GHz as a function of temperature. In the upper panel (a), the measurement of $\hat{Z}_{S\|}$ was done in the antinode of the electric field with $\mathbf{E}_{ac}$ parallel to the c direction. The lower panel (b) shows the temperature dependence of the out-of-plane surface impedance $\hat{Z}_{S\perp}$. This measurement was done in the antinode of the electric field with $\mathbf{E}_{ac}$ parallel to the a direction.

$\tau_{\|}$, the value of X_S is about 10% greater than R_S.

It is important to notice that in the temperature region below T_c, the "normal state" factor is defined by the temperature-independent value of σ_n fixed at a temperature point (9 K) slightly above T_c rather than the expected normal state conductivity $\sigma_n(T)$ [and consequently $R_n(T)$ and $X_n(T)$] which would be recovered at the same temperature. The temperature dependence of $\sigma_n(T)$ below T_c was measured by Achkir *et al.*[21] by applying a magnetic field of 10 T (well above H_{c2}) while performing similar surface impedance measurements at 17 GHz. The evaluation had to assume that the magnetoresistance found above T_c can be extrapolated to low temperatures. In continuation of the above-T_c temperature range, the overall resistivity behavior was found in agreement with the T^2 functional form discussed in Eq. (9). This indicates that the scattering rate $1/\tau(T)$ is temperature dependent, but rules out models predicting any drastic deviation from a shallow monotonic decrease of $1/\tau(T)$ in the region 0–9 K. However, the $\tau^{-1}(T) \propto T^2$ functional form will be included in the fit of the data.

The smooth onset and relatively broad transition observed in $(BEDT\text{-}TTF)_2Cu(NCS)_2$ can crudely be modeled along the lines which have been used for interpreting the specific heat[11] by assuming a distribution of local transition temperatures in the specimen. Such a distribution is expected also to influence the temperature dependence of the electrodynamical response. We have modeled this by assuming a Gaussian distribution of T_c with a standard deviation of 0.25. The solid lines in Fig. 4(a) are $X_S(T)$ and $R_S(T)$ resulting from this procedure. Although representing the broad transition with a simple distribution of independent local transition temperatures and calculating X_S and R_S is certainly an oversimplification, it is clear from Fig. 4 that one can account for the full in-plane electrodynamics with a BCS ground state and moderate sample quality. Another way to fit the

broad transition are fluctuation-based models, since fluctuation effects may occur near T_c for very anisotropic conductors. Indications of fluctuation effects were recently found by magnetization measurements.[46]

The temperature dependence of R_S and X_S below T_c = 8.2 K, obtained from a configuration where the electric field $\mathbf{E}_{ac}$ is parallel to the a direction (i.e., normal to the planes), is shown in Fig. 4(b). As for the parallel direction, all the data shown in Fig. 4(b) are normalized to the value of the surface resistance R_n at 9 K. Using the same type of analysis as in the parallel direction, we have fitted R_S and X_S in a consistent procedure discussed later. Again we have evaluated the temperature dependence of the scattering rate by fitting the normal state resistivity $\rho_n(T)$ above T_c by a second order polynomial fit [cf. Eq. (9)], and used this to estimate $\tau_\perp(T)$ in the temperature region below T_c.

Comparing the temperature dependence of the surface resistance R_S/R_n as measured with the **E** field along the a axis [$R_{S\perp}$, Fig. 4(a)] with the same measurement configuration but an **E** field oriented along the c axis [$R_{S\parallel}$, Fig. 4(b)] points out the perfect agreement of the two data sets, although the normal state values are very different.

2. κ-(BEDT-TTF)$_2$Cu[N(CN)$_2$]Br

The surface impedance of (BEDT-TTF)$_2$Cu[N(CN)$_2$]Br is shown in Fig. 6 normalized to the normal state surface resistance R_n at 13 K. The measurements were performed at 35 GHz with the electric field parallel to the plane. Similar experiments with the **H** field in the plane were conducted in order to probe the out-of-plane properties. Due to the high residual losses in the perpendicular direction, the resolution and consequently the scattering of these data are poor.

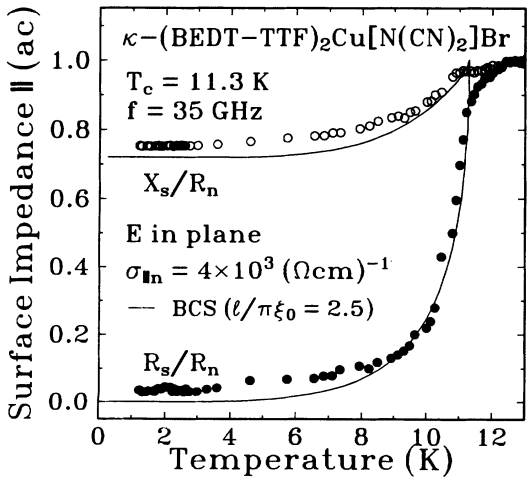

FIG. 6. The surface impedance $\hat{Z}_{S\parallel}$ of (BEDT-TTF)$_2$Cu[N(CN)$_2$]Br measured at a frequency of 35 GHz. The measurement was done in the antinode of the electric field with $\mathbf{E}_{ac}$ parallel to the ac planes.

Assuming that the Hagen-Rubens condition $\omega\tau \ll 1$ is fulfilled, we set $R_S = X_S$ slightly above T_c = 11.3 K [Eq. (5)]. In both directions our results can be well described by the BCS ground state using the parameters $2\Delta/k_BT_c = 5$ and $\ell_\parallel/(\pi\xi_{0\parallel}) = 2.5$ (as discussed later). Since the superconducting transition is sharp ($\Delta T_c \leq 0.3$ K), no smearing of the transition temperature was done in the fit. As for (BEDT-TTF)$_2$Cu(NCS)$_2$, we find a remarkable similarity in the overall shape of R_S and X_S in both directions even though the absolute value in the normal state $\sigma_n(T = 13\text{ K})$ is three orders of magnitude different.

C. Penetration depth

From Eq. (7) we see that the surface reactance X_S and therefore the measured frequency shift are directly proportional to the microwave penetration depth. Three configurations have been employed (Fig. 7). In one arrangement the ac magnetic field is directed perpendicular to the highly conducting plane. Consequently in this configuration the penetration depth in the highly conducting planes $\lambda_\parallel$ is measured, since the eddy currents are flowing in this plane. The same quantity is probed

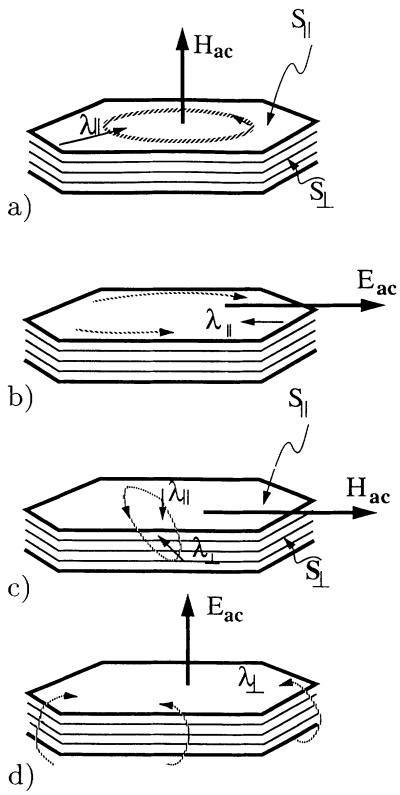

FIG. 7. Various configurations for measuring the penetration depth: (a) The magnetic field $\mathbf{H}_{ac}$ induces eddy currents in the planes and $\lambda_\parallel$ is probed. (b) The same quantity is measured with the electric field $\mathbf{E}_{ac}$ parallel to the layers. (c) With $\mathbf{H}_{ac}$ in the plane basically both $\lambda_\parallel$ and $\lambda_\perp$ are probed. (d) $\mathbf{E}_{ac}$ normal to the planes is sensitive to $\lambda_\perp$.

with the electric field in the plane. The relevant surface $S_\perp$ in both cases is the sum of the small sides around the sample. In the third configuration, the ac magnetic field is parallel to the highly conducting plane. In this configuration both the penetration depth along the layers $\lambda_\parallel$ and perpendicular to the layers $\lambda_\perp$ will contribute to the total frequency shift. Then the frequency shift due to the specimen is given by

$$\frac{\Delta f}{f_0} \propto (S_\perp \lambda_\parallel + S_\parallel \lambda_\perp), \tag{12}$$

where $S_\parallel$ is twice the area of the plane. Typically $\lambda_\perp \gg \lambda_\parallel$ and the contributions of the perpendicular orientation dominate.

1. κ-(BEDT-TTF)$_2$Cu(NCS)$_2$

The measured penetration depth of (BEDT-TTF)$_2$Cu(NCS)$_2$ in the two directions is displayed in Fig. 8 in comparison with published results. Since the evaluation of the sample geometry, and thus the resonator constant in Eq. (4), is difficult, the absolute value was obtained more accurately by using the skin depth $\delta = [2/(\mu_0 \omega \sigma_1)]^{1/2}$ of the normal state which is related to the surface reactance by Eq. (5): $\delta_\parallel(T = 9\ \mathrm{K}) = 4.4\ \mu\mathrm{m}$ and 3.4 μm at $f = 35$ GHz and 60 GHz, respectively. With the exception of Refs. 17 and 21, there is a good agreement between all the measurements. Even with the extended temperature range down to 0.8 K and the increased accuracy of $\delta\lambda/\lambda = \pm\ 0.007$, no indication of a temperature dependence can be found below $0.3T_c$. The absolute value of the zero temperature penetration depth measured at 35 GHz $\lambda_\parallel(T = 0) = 0.8\ \mu$m was found to be in good agreement with the literature values of 0.78 μm and 0.98 μm as obtained by μSR.[16,47] The analysis of our 60 GHz data in Fig. 4(a) leads to $\lambda_\parallel(T = 0) = 1.4\ \mu$m. The accordance with the μSR results also demonstrates that misalignment effects do not play an important role.

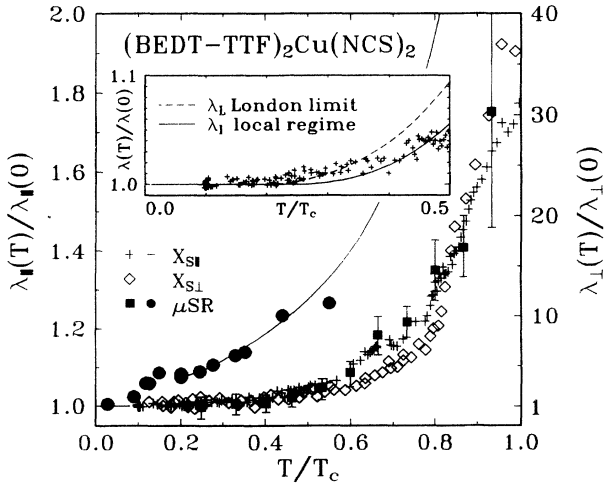

FIG. 8. Temperature dependence of the penetration depth of (BEDT-TTF)$_2$Cu(NCS)$_2$ measured at 35 GHz (pluses) and 60 GHz (open diamonds) in comparison with results from surface impedance experiments of Achkir *et al.* (Ref. 21) (solid line), and with μSR experiments of Harshman *et al.* (Ref. 16) (solid boxes) and Le *et al.* (Ref. 17) (solid circles). The experiments probe $\lambda_\parallel$, except for the open diamonds where $\lambda_\perp$ corresponds to the right axis. The inset demonstrates the agreement with the predictions of the BCS theory where the dashed line represents the London regime and the solid line the local regime.

For a finite mean free path $\ell = 150$ Å the measured penetration depth λ exceeds the London penetration depth λ_L:

$$\lambda(T = 0) = \lambda_L(T = 0)\left(1 + \frac{\xi_0}{\ell}\right)^{1/2}, \tag{13}$$

where $\xi_0 = 70$ Å is the coherence length and λ_L can be estimated from the normal state parameters:

$$\lambda_L(T = 0) = \left(\frac{m^*}{\mu_0 e^2 n}\right)^{1/2}. \tag{14}$$

From this we obtain $\lambda_L(T = 0) = 0.79\ \mu$m and consequently $\lambda(T = 0) = 0.95\ \mu$m, which agrees well with our experimental data.

The similar temperature dependence was obtained in the configuration with the **H** field parallel to the c direction,[18] and yields a low temperature value of $\lambda_\perp(T = 0) = 40\ \mu$m. Perpendicular to the plane, the coherence length $\xi_{0\perp} < s$, where $s = 15.2$ Å is the interplane separation, and $\xi_{0\perp} = 5$ Å is the coherence length.[48] Under such circumstances, the situation is close to that of Josephson coupled layers, with the resulting penetration depth

$$\lambda_\perp = \left[\frac{\hbar c^2 \rho_\perp}{4\pi^2 \Delta}\right]^{1/2}, \tag{15}$$

where $\rho_\perp$ is the resistivity perpendicular to the planes. Using $\rho_\perp(T = 9\ \mathrm{K}) = 0.25\ \Omega$cm from our surface resistance measurements and the weak coupling gap, this leads to $\lambda_\perp = 32\ \mu$m in excellent agreement with the experimentally obtained values.

In the inset of Fig. 8, the measured results of the normalized penetration depth $\lambda(T)$ are compared with theoretical predictions of the weak coupling BCS theory. The solid line represents the local regime ($\lambda > \xi_0 > \ell$); the dashed line is the London limit ($\lambda > \ell > \xi_0$). From our penetration depth data we cannot distinguish between clean ($\ell > \xi_0$) and the dirty ($\xi_0 > \ell$) limits.

2. κ-(BEDT-TTF)$_2$Cu[N(CN)$_2$]Br

The penetration depth for (BEDT-TTF)$_2$Cu[N(CN)$_2$]Br as a function of the reduced temperature T/T_c is shown in Fig. 9. The measurement was performed at 35 GHz with the **E** field oriented parallel to the (ac) planes; therefore $\lambda_\parallel(T)$ was probed. The temperature dependence agrees with the results of re-

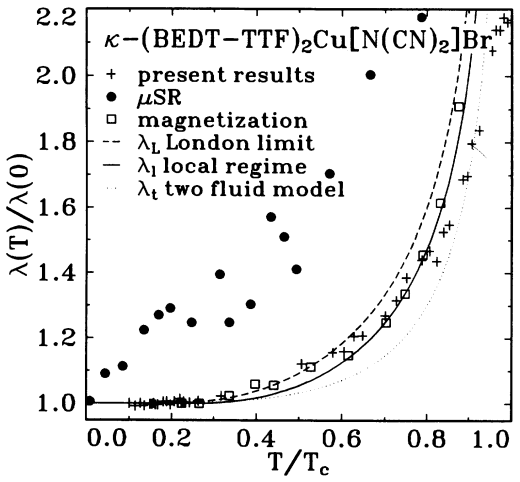

FIG. 9. The penetration depth $\lambda_{\|}$ in (BEDT-TTF)$_2$Cu[N(CN)$_2$]Br as a function of temperature. The solid circles show μSR data (Ref. 17) and the open boxes results from measurements of the magnetization (Ref. 14). The dashed line is the BCS weak coupling limit, the solid line represents the local regime, and the dotted line gives the results of the two-fluid model which are close to the strong coupling limit.

versible magnetization experiments[14] and is in accordance with calculations based on the BCS theory either in the local regime (dashed line) or the London limit (solid line). The dotted line corresponds to the two-fluid model $\lambda_T(T) = \lambda_0[1 - (T/T_c)^4]^{-1/2}$ which is close to strong coupling calculations. Lang *et al.*[14] found that in the temperature range below T_c ($T > 0.6T_c$) their penetration depth data lie below the prediction of the weak coupling BCS limit. They interpret this as an indication of moderate or strong coupling. Our data do not contradict their conclusion.

Instead of estimating the surface area of our samples, we used the skin depth at 13 K in order to normalize our experimental data. From our 35 GHz surface resistance measurements we get $\delta_{\|} = 4.2$ μm and $\delta_{\perp} = 100$ μm. The resulting absolute value of the zero temperature penetration depth $\lambda_{\|}(T = 0) = 1.5$ μm is in fair accordance with μSR (Ref. 17) and magnetization[14] results (0.84 μm and 0.78 μm). Perpendicular to the plane we estimate $\lambda_{\perp}(T = 0) = 38$ μm from our surface reactance measurements. We stayed well below the upper limit of 220 μm set by the ac susceptibility measurements of Takahashi *et al.*[8]

D. Complex superconducting conductivity

By Eq. (2), both the surface resistance and surface reactance depend on the parameters σ_1 and σ_2 which determine the superconducting state. The complex conductivity $\hat{\sigma}(T)$ in the superconducting state can therefore be evaluated using the experimentally accessible R_S and X_S as input parameters:

$$\sigma_1 = \frac{2\mu_0\omega R_S X_S}{(R_S^2 + X_S^2)^2} \quad \text{and} \quad \sigma_2 = \frac{\mu_0\omega(X_S^2 - R_S^2)}{(R_S^2 + X_S^2)^2}. \quad (16)$$

1. κ-(BEDT-TTF)$_2$Cu(NCS)$_2$

In Fig. 10 the complex conductivity parallel and perpendicular to the planes of (BEDT-TTF)$_2$Cu(NCS)$_2$ is displayed as a function of temperature. For a BCS superconductor in the dirty limit [i.e., $\ell/(\pi\xi_0) \ll 1$] the equations for the temperature- and frequency-dependent response of $\hat{\sigma}$ were worked out by Mattis and Bardeen.[49] As pointed out before, this limit may not be appropriate for (BEDT-TTF)$_2$Cu(NCS)$_2$ since the normal state dc conductivity and optical relaxation time yield a mean free path $\ell_{\|} \approx 150$ Å at 10 K; the coherence length is[48] $\xi_{0\|} = 70$ Å. Consequently we went beyond Mattis and Bardeen and performed calculations similar to Chang and Scalapino,[50] assuming a two-dimensional BCS ground state. We restricted ourselves to the weak coupling limit $\Delta = 1.76k_BT_c$ and fitted our results for

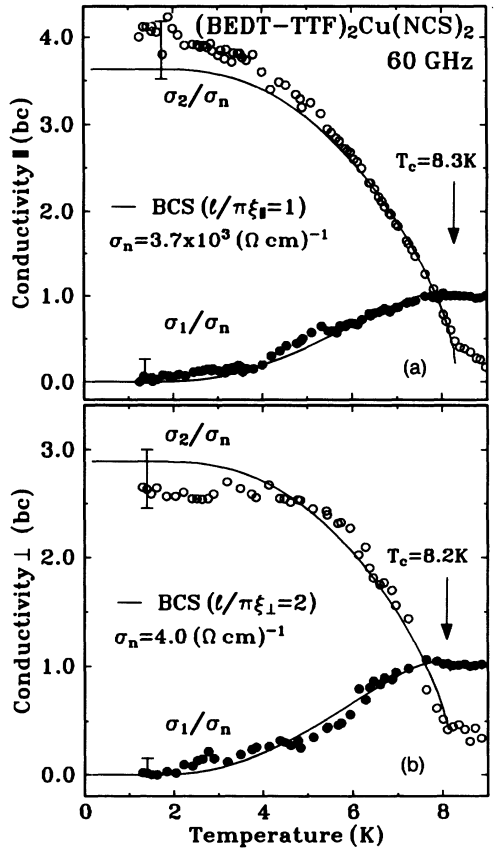

FIG. 10. Temperature dependence of the normalized components σ_1 and σ_2 of the optical conductivity at 60 GHz both (a) parallel and (b) perpendicular to the highly conducting layers of (BEDT-TTF)$_2$Cu(NCS)$_2$. The solid lines represent the results of BCS theory with $\ell/\pi\xi_0 = 1$ and 2, respectively.

various values of the only remaining parameter $\ell/(\pi\xi_0)$.

In Fig. 10(a) we display both components of the complex conductivity σ_1 and σ_2 in the highly conducting (bc) plane, normalized to the normal state value at $T = 9$ K. The same parameters are plotted in Fig. 10(b) for the direction perpendicular to the plane. The best fit to our data at 60 GHz (Fig. 4) was obtained with $\ell_\parallel/(\pi\xi_{0\parallel}) = 1$; i.e., $\omega\tau_\parallel = 0.18$ at $f = 60$ GHz and the relaxation rate $1/2\pi\tau_\parallel = 15$ cm^{-1} at 10 K. The solid line includes the temperature dependence effects of the scattering rate [$\tau^{-1}(T) \propto T^2$]. For the 35 GHz measurement (Fig. 5), we fit the data with $\ell_\parallel/(\pi\xi_{0\parallel}) = 0.7$; consequently the relaxation rate $1/2\pi\tau_\parallel = 16$ cm^{-1}. These values for the scattering rate are significantly smaller than 1000 cm^{-1} obtained from optical studies if the reflectivity dip in the midinfrared is fitted. It is slightly below 50 cm^{-1} which was obtained by modeling the Drude peak in the far-infrared,[37] and it is somewhat larger than 2 cm^{-1} which is the result of Shubnikov–de Haas measurements.[2] Some of these differences may reflect a frequency-dependent relaxation time and deviations from a simple Drude response in the metallic state.

The values for the perpendicular direction are $\ell_\perp/(\pi\xi_{0\perp}) = 2$ which yields $\ell_\perp = 30$ Å, using $\xi_{0\perp} = 5$ Å. The Fermi velocity may be estimated from the definition of the coherence length:

$$\xi_0 = \frac{\hbar v_F}{\pi\Delta}. \tag{17}$$

We obtain $v_F = 4.4\times10^6$ cm/s in the plane (in agreement with the value obtained above from the Fermi surface area) and $v_F = 3.1 \times 10^6$ cm/s normal to the plane. From the latter value the scattering rate is calculated to be $1/(2\pi\tau_\perp) = 5$ cm^{-1}.

2. κ-(BEDT-TTF)$_2$Cu[N(CN)$_2$]Br

Applying Eq. (16) to our 35 GHz results, we calculated the complex conductivity of (BEDT-TTF)$_2$Cu[N(CN)$_2$]Br (Fig. 11). By comparing the results with the predictions of a two-dimensional BCS ground state[50] we reached a fair agreement in the weak coupling limit ($2\Delta/k_BT_c = 3.53$) using $\ell/\pi\xi_0 = 2$ (dashed line). A much better fit (solid line) can be obtained using a larger gap value of $2\Delta/k_BT_c = 5$ and $\ell/\pi\xi_{0\parallel} = 2.5$. This is in accordance with results from dc magnetization experiments[14] which indicated strong or medium coupling effects in (BEDT-TTF)$_2$Cu[N(CN)$_2$]-Br.

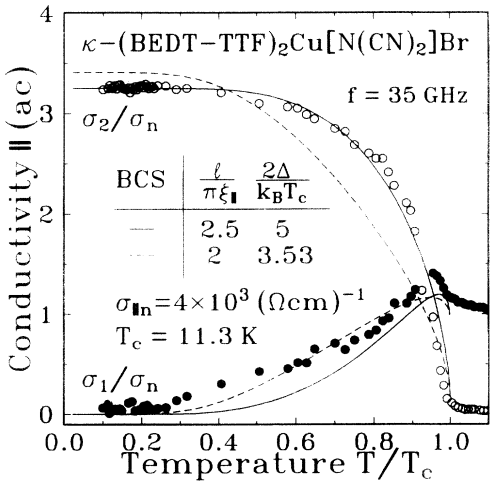

FIG. 11. The normalized conductivity σ_1 and σ_2 of (BEDT-TTF)$_2$Cu[N(CN)$_2$]Br at 35 GHz parallel to the highly conducting layers plotted as function of the reduced temperature T/T_c. The dashed lines represent the results of BCS theory with a gap $2\Delta = 3.53k_BT_c$, while a larger single particle gap $2\Delta = 5k_BT_c$ was assumed for calculating the solid lines.

Using the literature value[51] of the coherence length obtained from upper critical field studies $\xi_{0\parallel} = 37$ Å we calculate $\ell_\parallel = 290$ Å in the parallel direction and consequently $1/(2\pi\tau_\parallel) = 30$ cm^{-1}. The fact that no deviation from the Hagen-Rubens limit was observed is in agreement with $\omega\tau_\parallel = 0.04 \ll 1$. The out-of-plane results can be fit by $\ell/(\pi\xi_{0\perp}) = 4$, from which we obtain $\ell_\perp = 50$ Å with $\xi_{0\perp} = 4$ Å.[51] Calculating the Fermi velocity from Eq. (17), $v_F = 4.7\times10^5$ cm/s, and we find $1/(2\pi\tau_\perp) = 5$ cm^{-1}.

In Table I we collect the results obtained from our microwave surface impedance measurements on κ-(BEDT-TTF)$_2$Cu(NCS)$_2$ at 60 GHz together with the 35 GHz results on κ-(BEDT-TTF)$_2$Cu[N(CN)$_2$]Br. Also included are parameters from Refs. 48 and 51 on the coherence length.

TABLE I. Electrodynamical properties of (BEDT-TTF)$_2$Cu(NCS)$_2$ measured at 60 GHz, and (BEDT-TTF)$_2$Cu[N(CN)$_2$]Br measured at 35 GHz with the current flowing either parallel or perpenduclar to the highly conducting plane.

κ-(BEDT-TTF)$_2X$ $X =$		T_c [K]	$\sigma_n(T = 300$ K) [$(\Omega$ cm$)^{-1}$]	$\sigma_n(T > T_c)$ [$(\Omega$ cm$)^{-1}$]	δ [μm]	λ [μm]	ℓ [Å]	ξ [Å]	$1/(2\pi\tau)$ [cm^{-1}]	2Δ [cm^{-1}]
Cu(NCS)$_2$	$\parallel$	8.3	20	3.7×10^3	3.4	1.4	150	70	15	21
	$\perp$	8.2	2.0×10^{-3}	4.0	100	40	30	5	5	21
Cu[N(CN)$_2$]Br	$\parallel$	11.3	23	4.0×10^3	4.2	1.5	290	37	30	40
	$\perp$	11.3	0.5	6.4	110	38	50	6	5	40

IV. DISCUSSION

The resistivity of κ-(BEDT-TTF)$_2$Cu(NCS)$_2$ in the millimeter wave frequency range is very similar in absolute value and temperature dependence to the one for direct current. Only slightly above T_c are small deviations from the Hagen-Rubens condition seen. From our analysis of the 60 GHz data we estimate $1/(2\pi\tau_{\|}) = 15$ cm^{-1} parallel to the (bc) planes. On the one hand the value has to be compared with the relaxation rate 1000 cm^{-1} resulting from the fit of the midinfrared optical reflectivity and 50 cm^{-1} if just the far-infrared Drude contribution is taken into account.[37] On the other hand, Shubnikov–de Haas experiments[2] lead to a value of $1/(2\pi\tau_{\|}) = 2$ cm^{-1}.

From our surface impedance measurements of κ-(BEDT-TTF)$_2$Cu[N(CN)$_2$]Br at a frequency of 35 GHz we find a scattering rate $1/(2\pi\tau) = 30$ cm^{-1}. This is in good agreement with the width of the Drude peak [(20 ± 5) cm^{-1}] determined from the low frequency optical conductivity.[40] Since the midinfrared reflectivity is similar in both (BEDT-TTF)$_2$Cu(NCS)$_2$ and (BEDT--TTF)$_2$Cu[N(CN)$_2$]Br, a Drude fit of the entire infrared spectrum also leads to a relaxation rate of ~ 1000 cm^{-1}. We feel that the small differences in parameters extracted from the studies of both compounds do not reflect different intrinsic properties but are due to the quality of the samples. The main features of the normal state electrodynamics are identical: a fairly good conductor with a semiconductor like resistivity above 100 K and a T^2-temperature dependence below. The scattering rate is about 20 cm^{-1} when probed with microwaves, but seems to depend on the measurement frequency. From this we infer that the simple Drude model does not apply.

The temperature dependence of the penetration depth is a direct indication of the pairing mechanism. Since $\lambda(T)$ is governed by the quasiparticle excitation spectrum, zeros of the order parameter should result in an anisotropical and power-law T dependence of $\lambda(T \to 0)$ due to the enhanced pair-breaking excitations at low temperatures. While triplet pairing results in a linear temperature dependence,[52] s-wave pairing leads to a flat behavior with $d\lambda(T)/dT\ |_{T\to 0} = 0$. It is clear from inset of Fig. 8 that in both directions $\lambda(T)$ is well described by assuming a singlet ground state. The resolution of our measurement does not allow us to distinguish between different coupling limits as Lang *et al.*[14] were able to do in their magnetization studies. They conclude (BEDT-TTF)$_2$Cu(NCS)$_2$ is in the weak coupling limit while (BEDT-TTF)$_2$Cu[N(CN)$_2$]Br seems to be medium coupling, but for both compounds perfect agreement with s-wave pairing was found. Based on the μSR data of Le *et al.*,[17] Achkir *et al.*[21] extrapolated the penetration depth linearly to low temperatures although their surface reactance data leave room for a conventional interpretation in accordance with our results. The deviating results may be due to an extrinsic defect-mediated screening mechanism which gives rise to an enhanced penetration depth. The experimentally determined[53] temperature dependence $\lambda(T)/\lambda(0) = (1-t^2)^{-1} \approx 1 + t^2$ of this vortex-pair nucleation at defects can easily be mistaken for evidence of nonconventional pairing.

It is obvious from Figs. 10 and 11 that the normalized behavior of the electrodynamical response is highly similar in both orientations, parallel to the highly conducting plane as well as perpendicular to it, despite the fact that the normal state values differ by several orders of magnitude between the two configurations. The similarity between the different crystallographic orientations suggests isotropic pairing. Both of our results are in full agreement with a BCS ground state.

In the dirty limit ($\xi_0 > \ell$) the imaginary part of the conductivity σ_2 is related to the superconducting energy gap:[36]

$$\frac{\sigma_2(\omega,T)}{\sigma_n} = \frac{\pi\Delta(T)}{\hbar\omega}\tanh\left[\frac{\Delta(T)}{2k_BT}\right] \approx \lim_{T\to 0}\frac{\pi\Delta(T=0)}{\hbar\omega}. \tag{18}$$

In the clean limit, however, σ_2/σ_n tends to the ratio $1/\omega\tau$ at low temperatures, and so in our case we cannot extract Δ from the zero temperature value of σ_2, though we can check the consistency as far as the crossover from the Hagen-Rubens regime ($\omega\tau < 1$) to the relaxation regime ($\omega\tau > 1$) is concerned. The comparison of mean free path and coherence length indicates that both organic superconductors (BEDT-TTF)$_2$Cu(NCS)$_2$ and (BEDT-TTF)$_2$Cu[N(CN)$_2$]Br are right at the boundary between the dirty and clean regimes, slightly on the latter side. This may explain the null result in the search for the single particle gap by optical absorption methods.[45]

The dominant feature of the σ_1 curve is the peak below the superconducting transition temperature (Figs. 10 and 11), which finds a natural explanation in the BCS model: The broad maximum reflects the case-II coherence factor.[36] The coherence peak is caused by the divergency of the excitation density of states at the gap edge plus the coherence factor. The photon energy smooths out this singularity and is responsible for the reduced height of the peak feature for this relatively small T_c compound (the size of the peak goes as $\ln\frac{2\Delta}{\hbar\omega}$). At 60 GHz the photon energy becomes comparable to the single particle gap Δ, and the peak is almost smeared out. The experiments on (BEDT-TTF)$_2$Cu(NCS)$_2$ performed at 35 GHz exhibit a peak value of $\sigma_1/\sigma_n \approx 1.35$, again in excellent agreement with the BCS theory.[23] Since we observe the same temperature dependence for $\sigma_1(T)$ both parallel and perpendicular to the planes, we deduce that the divergency in the optical response of the system is identical at various orientations. We conclude that the ratio $\Delta/\hbar\omega$ is a fundamental constant of the superconducting phase and thus the gap is isotropic for all three crystallographic axes. Even if we do not measure the single particle gap Δ directly, we are able to fit the results in both directions with the same value. For κ-(BEDT–TTF)$_2$Cu(NCS)$_2$ we find $2\Delta = 3.53k_BT_c = 20$ cm^{-1}, while a larger gap is obtained in κ-(BEDT--TTF)$_2$Cu[N(CN)$_2$]Br: $2\Delta = 5k_BT_c = 40$ cm^{-1}. Indications of this difference were seen in magnetization measurements.[14] Results of the specific heat studies imply that both compounds are strong coupling superconductors.[54,55]

It is expected that the singularity in the density of

states is removed for d-wave pairing leading to a sharp decrease of the optical conductivity. Consequently higher momentum pairing leads to the rapid disappearance of the coherence peak and is expected to give σ_1 values significantly below the solid line in Figs. 10 and 11. As a consequence, for d-wave pairing the gap should have vanished along the direction normal to the plane.

Recent microwave experiments at 17 GHz by Achkir *et al.*[21] basically produce similar results for $\sigma_{1\|}$. The interpretation, however, is contrary, since the authors oppose the application of the BCS theory and apply an inelastic scattering term $1/\tau_{\text{ine}}$, with $1/\tau = 1/\tau_0 + 1/\tau_{\text{ine}}$, in order to explain the observed peak. From this point of view, the maximum of $\sigma_1(T)$ is the result of the increasing inelastic scattering time τ_{ine} and, using the two-fluid picture, the disappearance of normal carriers (deduced from the decreasing penetration depth λ) as the temperature decreases. We have recently demonstrated[56] that the electrodynamics of a superconductor cannot be simply written as the sum of the condensed and uncondensed electrons. Applying the same analysis on a conventional superconductor leads to an unexpected rapid decrease of $1/\tau$ below T_c. The low temperature resistance of the normal state, measured in a large magnetic field of 10 T,[21] gives no indication of a rapid change in the scattering rate. We feel that our results as well as the results of Achkir *et al.* can be explained within BCS theory, by assuming a smearing of the transition and deviation from the Hagen-Rubens limit $\omega\tau \ll 1$.

V. CONCLUSION

In the temperature region above T_c (but $T <$ 100 K) both materials behave like metals with a scattering rate of approximately 20 cm^{-1}. The penetration depth $\lambda(T)$ of the two organic superconductors κ-(BEDT-TTF)$_2$Cu(NCS)$_2$ and κ-(BEDT-TTF)$_2$Cu[N(CN)$_2$]Br shows a flat behavior for low temperatures. This $\lim_{T\to 0} d\lambda(T)/dT = 0$ is in agreement with the BCS prediction and conventional s-wave pairing. The similar temperature dependence of $\hat{\sigma}/\sigma_n$ in both directions parallel to the planes and perpendicular to the planes indicates isotropic pairing. The coherence peak in σ_1 below T_c rules out a superconducting ground state which is significantly different from singlet pairing. We conclude that our surface impedance measurements on both κ-(BEDT–TTF)$_2$Cu(NCS)$_2$ and κ-(BEDT–TTF)$_2$Cu[N(CN)$_2$]Br can be described in all respects by BCS theory.

ACKNOWLEDGMENTS

The first samples for this study were provided by F. Wudl. This work was supported by the INCOR program of the University of California and by DARPA. The work at Argonne National Laboratory was supported by the Office of Basic Energy Sciences, Division of Materials Sciences, of the U.S. Department of Energy, Contract No. W-31-109-ENG-38. One of us (M.D.) acknowledges support of the Alexander von Humboldt Foundation.

* Present address: Department of Physics, Massachusetts Institute of Technology, Cambridge, MA 02139.

[1] J. M. Williams, J. R. Ferraro, R. J. Thorn, K. D. Carlson, U. Geiser, H. H. Wang, A. M. Kini, and M. H. Whangbo, *Organic Superconductors* (Prentice Hall, Englewood Cliffs, NJ, 1992).

[2] N. Toyota, T. Sasaki, K. Murata, Y. Honda, M. Tokumoto, H. Bando, N. Kinoshita, H. Anzai, T. Ishiguro, and Y. Muto, J. Phys. Soc. Jpn. **57**, 2616 (1988).

[3] H. Urayama, H. Yamochi, G. Saito, K. Nozawa, T. Sugano, M. Kinoshita, S. Sato, K. Oshima, A. Kawamoto, and J. Tanaka, Chem. Lett. **1988**, 55 (1988).

[4] L. I. Buravov, A. V. Zvarykina, N. D. Kushch, V. N. Laukhin, V. A. Merzhanov, A. G. Khomenko, and E. B. Yagubskii, Sov. Phys. JETP **68**, 182 (1989).

[5] L. I. Buravov, N. D. Kushch, V. A. Merzhanov, M. V. Osherov, A. G. Khomenko, and E. B. Yagubskii, J. Phys. I (France) **2**, 1257 (1992).

[6] K. Oshima, H. Urayama, H. Yamochi, and G. Saito, J. Phys. Soc. Jpn. **57**, 730 (1988).

[7] T. Takahashi, T. Tokiwa, K. Konoda, H. Urayama, H. Yamochi, and G. Saito, Physica C **153-155**, 487 (1988).

[8] T. Takahashi, K. Kanoda, and G. Saito, Jpn. J. Appl. Phys. **7**, 414 (1992).

[9] S. M. DeSato, C. P. Schlichter, H. H. Wang, U. Geiser, and J. M. Williams, Phys. Rev. Lett. **70**, 2956 (1993).

[10] S. Katsumoto, S. Kobayashi, H. Urayama, H. Yamochi, and G. Saito, J. Phys. Soc. Jpn. **57**, 3672 (1988).

[11] J. Graebner, R. C. Haddon, S. V. Chichester, and S. H. Glarum, Phys. Rev. B **41**, 4808 (1990).

[12] K. Kanoda, K. Akiba, K. Suzuki, and T. Takahashi, Phys. Rev. Lett. **65**, 1271 (1990).

[13] M. Lang, N. Toyota, T. Sasaki, and H. Sato, Phys. Rev. Lett. **69**, 1443 (1992).

[14] M. Lang, N. Toyota, T. Sasaki, and H. Sato, Phys. Rev. B **46**, 5822 (1992).

[15] S. Sridhar, B. Mahe, B. A. Willemsen, D. H. Wu, and R. C. Haddon, Phys. Rev. Lett. **68**, 2220 (1992).

[16] D. R. Harshman, R. N. Kleiman, R. C. Haddon, S. V. Chichester-Hicks, M. L. Kaplan, L. W. Rupp, T. Pfiz, D. L. Williams, and D. B. Mitzi, Phys. Rev. Lett. **64**, 1293 (1990).

[17] L. P. Le *et al.*, Phys. Rev. Lett. **68**, 1923 (1992).

[18] K. Holczer, D. Quinlivan, O. Klein, G. Grüner, and F. Wudl, Solid State Commun. **76**, 499 (1990).

[19] O. Klein, K. Holczer, G. Grüner, J. J. Chang, and F. Wudl, Phys. Rev. Lett. **66**, 655 (1991).

[20] M. Dressel, L. Degiorgi, O. Klein, and G. Grüner, J. Phys. Chem. Solids **54**, 1411 (1993).

[21] D. Achkir, M. Poirier, C. Bourbonnais, G. Quirion, C. Lenior, P. Batail, and D. Jérome, Phys. Rev. B **47**, 11595 (1993).

[22] K. Holczer, O. Klein, G. Grüner, H. Yamochi, and F. Wudl, in *Organic Superconductivity*, edited by V. Z. Kresin and W. A. Little (Plenum Press, New York, 1990), p. 81.

[23] M. Dressel, S. Bruder, G. Grüner, K. Carlson, H. Wang,

and J. Williams, Phys. Rev. B **48**, 9906 (1993).
[24] M. Dressel, O. Klein, S. Donovan, and G. Grüner, Int. J. Infrared Millimeter Waves **14**, 2489 (1993).
[25] A. M. Kini *et al.*, Inorg. Chem. **29**, 2555 (1990).
[26] H. H. Wang *et al.*, Chem. Mater. **2**, 482 (1990).
[27] O. Klein, S. Donovan, M. Dressel, and G. Grüner, Int. J. Infrared Millimeter Waves **14**, 2423 (1993).
[28] S. Donovan, O. Klein, M. Dressel, K. Holczer, and G. Grüner, Int. J. Infrared Millimeter Waves **14**, 2459 (1993).
[29] L. Buranov and I. Shchegolev, Prib. Tech. Eksp. **2**, 171 (1971) [Instr. Exp. Techn. **14**, 528 (1971)].
[30] J. Osborn, Phys. Rev. **67**, 351 (1945).
[31] M. Tokumoto, in *The Physics and Chemistry of Organic Superconductors*, edited by G. Saito and S. Kagoshima (Springer Verlag, Berlin, 1990), p. 116.
[32] Y. Ueba, T. Mishima, H. Kusuhara, and K. Tada, in *The Physics and Chemistry of Organic Superconductors*, edited by G. Saito and S. Kagoshima (Springer-Verlag, Berlin, 1990), p. 284.
[33] H. Müller, C. P. Heidmann, W. Biberacher, and K. Andres, Synth. Met. **41-43**, 1943 (1991).
[34] D. Schweitzer (private communication).
[35] S. E. Schirber, E. L. Venturini, A. M. Kini, H. H. Wang, J. R. Whitworth, and J. M. Williams, Physica C **152**, 157 (1988).
[36] M. Tinkham, *Introduction to Superconductivity* (McGraw-Hill, New York, 1975).
[37] K. Kornelsen, J. E. Eldridge, C. C. Homes, H. H. Wang, and J. M. Williams, Solid State Commun. **72**, 475 (1989).
[38] K. Oshima, T. Mori, H. Inokuchi, H. Urayama, H. Yamochi, and G. Saito, Phys. Rev. B **38**, 938 (1988).
[39] J. Wosnitza, G. Crabtree, H. H. Wang, K. D. Carlson, M. D. Vashon, and J. M. Williams, Phys. Rev. Lett. **67**, 263 (1991).
[40] J. Eldridge, K. Kornelsen, H. Wang, J. Williams, A. D. Crouch, and D. Watkins, Solid State Commun. **79**, 583 (1991).
[41] M. H. Whangbo, J. J. Novoa, D. Jung, J. M. Williams, A. M. Kini, H. H. Wang, U. Geiser, M. A. Beno, and K. D. Carlson, in *Organic Superconductivity*, edited by V. Z. Kresin and W. A. Little (Plenum Press, New York, 1990), p. 243.
[42] H. Ito, M. Watanabe, Y. Nogami, T. Ishiguro, T. Komatsu, G. Saito, and N. Hosoito, J. Phys. Soc. Jpn. **60**, 3230 (1991).
[43] Y. Maruyama, T. Inabe, H. Urayama, H. Yamochi, and G. Saito, Solid State Commun. **67**, 163 (1988).
[44] H. Bando, S. Kashiwaya, T. Tokumoto, H. Anzai, N. Kinoshita, M. Tokumoto, and K. M. and K. Kajimura, in *The Physics and Chemistry of Organic Superconductors*, edited by G. Saito and S. Kagoshima (Springer-Verlag, Berlin, 1990), p. 167.
[45] K. Kornelsen, J. E. Eldridge, H. H. Wang, and J. M. Williams, Solid State Commun. **76**, 1009 (1990)
[46] M. Lang, F. Steglich, N. Toyota, and T. Sasaki, Phys. Rev. B **49**, 15227 (1994).
[47] Y. J. Uemura, L. P. Le, G. M. Luke, B. J. Sternlieb, J. H. Brewer, T. M. Riseman, G. Saito, and H. Yamochi, in *Organic Superconductivity*, edited by V. Kresin and W. Little (Plenum Press, New York, 1990), p. 23.
[48] G. Saito, Physica C **162-164**, 577 (1989).
[49] D. Mattis and J. Bardeen, Phys. Rev. **111**, 412 (1958).
[50] J. Chang and D. Scalapino, Phys. Rev. B **40**, 4299 (1989).
[51] W. K. Kwok *et al.*, Phys. Rev. B **42**, 8686 (1990).
[52] F. Gross, B. S. Chandrasekhar, D. Einzel, K. Andres, P. J. Hirschfeld, H. R. Ott, J. Beuers, Z. Fisk, and J. Smith, Z. Phys. B **64**, 175 (1986).
[53] A. F. Hebard, A. T. Fiory, M. P. Siegal, J. M. Phillips, and R. C. Haddon, Phys. Rev. B **44**, 9753 (1991).
[54] B. Andraka, J. S. Kim, G. R. Steward, K. D. Carlson, H. H. Wang, and J. M. Williams, Phys. Rev. B **40**, 11345 (1989).
[55] B. Andraka, C. S. Lee, J. S. Kim, G. R. Steward, K. D. Carlson, H. H. Wang, A. V. S. Crouch, A. M. Kini, and J. M. Williams, Solid State Commun. **79**, 57 (1991).
[56] O. Klein, E. J. Nicol, K. Holczer, and G. Grüner, Phys. Rev. B **50**, 6307 (1994).